NeuroImage 178 (2018) 1–10

Contents lists available at ScienceDirect

NeuroImage

journal homepage: www.elsevier.com/locate/neuroimage

Feasibility of imaging evoked activity throughout the rat brain using electrical impedance tomography

Mayo Faulkner *, Sana Hannan, Kirill Aristovich, James Avery, David Holder

University College London, London WC1E 6BT, UK

ARTICLE INFO

Keywords:
Electrical impedance tomography
Evoked potentials
Cortex
VPL
Fast neural EIT
Rat

ABSTRACT

Electrical Impedance Tomography (EIT) is an emerging technique which has been used to image evoked activity during whisker displacement in the cortex of an anaesthetised rat with a spatiotemporal resolution of 200 μm and 2 ms. The aim of this work was to extend EIT to image not only from the cortex but also from deeper structures active in somatosensory processing, specifically the ventral posterolateral (VPL) nucleus of the thalamus. The direct response in the cortex and VPL following 2 Hz forepaw stimulation were quantified using a 57-channel epicortical electrode array and a 16-channel depth electrode. Impedance changes of $-0.16 \pm 0.08\%$ at 12.9 ± 1.4 ms and $-0.41 \pm 0.14\%$ at 8.8 ± 1.9 ms were recorded from the cortex and VPL respectively. For imaging purposes, two 57-channel epicortical electrode arrays were used with one placed on each hemisphere of the rat brain. Despite using parameters optimised toward measuring thalamic activity and undertaking extensive averaging, reconstructed activity was constrained to the cortical somatosensory forepaw region and no significant activity at a depth greater than 1.6 mm below the surface of the cortex could be reconstructed. An evaluation of the depth sensitivity of EIT was investigated in simulations using estimates of the conductivity change and noise levels derived from experiments. These indicate that EIT imaging with epicortical electrodes is limited to activity occurring 2.5 mm below the surface of the cortex. This depth includes the hippocampus and so EIT has the potential to image activity, such as epilepsy, originating from this structure. To image deeper activity, however, alternative methods such as the additional implementation of depth electrodes will be required to gain the necessary depth resolution.

Introduction

A plethora of techniques have been developed to record and image neuronal networks in the brain to gain a better understanding of the underlying mechanisms and interactions that drive complex cognitive and behavioral tasks. Among the most promising include optical imaging techniques that can achieve single-cell resolution by implementing genetically encoded fluorescent indicators of membrane voltage or calcium concentration (Hillman, 2007; Lin and Schnitzer, 2016). Even with the most advanced optical microscopes, however, the field of view is restricted to 1 mm^3 and imaging is limited to depths of 1 mm (Ahrens et al., 2013; Helmchen and Denk, 2005; Theer and Denk, 2006). Densely populated micro-electrode arrays can be used to record local field potentials (LFP) and multi-unit activity (MUA) from neurons (Berényi et al., 2014; Buzsáki, 2004; Raducanu et al., 2017). An analysis of the spectral coherence between LFPs can elucidate the coupling between oscillatory signals in different brain regions (Friston et al., 2015; Gregoriou et al., 2009; Lowet et al., 2016). Multi-electrode arrays, however, can only detect from neurons located around 100 μm away (Kajikawa and Schroeder, 2011) and are inherently invasive. To non-invasively image connections between distinct brain areas, fMRI is currently the method of choice. Rather than direct activity, however, fMRI measures the epiphenomenal blood flow (Ogawa et al., 1990). EEG inverse source localisation can image direct neural activity over large regions of the brain. However, it has a low spatial resolution (Burle et al., 2015; Nunez et al., 1994) and is blind to dipole sources oriented tangentially to recording electrodes (Ahlfors et al., 2010; Hunold et al., 2016). Currently no satisfactory method exists to record direct neural activity occurring over large regions of the brain.

Electrical impedance tomography (EIT) is an imaging technique which has the potential to image neural activity occurring on the millisecond timescale throughout the brain. In EIT, multiple transfer impedance measurements are conducted using non-penetrating surface electrodes in order to reconstruct images of conductivity changes

* Corresponding author.
E-mail address: mayo.faulkner@ucl.ac.uk (M. Faulkner).

https://doi.org/10.1016/j.neuroimage.2018.05.022
Received 12 February 2018; Received in revised form 26 April 2018; Accepted 8 May 2018
Available online 10 May 2018

within a subject. A single transfer impedance measurement involves injecting current between a pair of electrodes and recording the resulting voltage on the remaining electrodes. Multiple transfer impedance measurements are obtained through the use of a switch network which allows current to be sequentially injected through different electrode pairs. Fast neural EIT can detect impedance changes associated with ion channel opening during neuronal depolarisation (Klivington and Galambos, 1967; Oh et al., 2011; Velluti et al., 1968). Impedance changes arise as injected current, normally confined to the extracellular space due to the high membrane capacitance of neurons, can pass through open ion channels in the membrane and additionally travel in the intracellular space. EIT has been used to produce images of cortical neural activity in an anaeasthetised rat during evoked activity (Aristovich et al., 2016) and during chemically induced epileptic interictal spikes (Vongerichten et al., 2016).

The sensitivity of EIT to conductivity changes is known to decrease with distance from the electrodes as the current density magnitude dissipates (Alessandrini and Scapin, 2017). The depth sensitivity can be augmented, however, through careful choice of the electrode positions, the electrode pairs through which current is injected (commonly termed the protocol), the frequency of injected current and the current amplitude. Thus far EIT imaging in the rat brain has been conducted using a 30-channel electrode array and this has limited the depth resolution to the cortex. Developments in the electrode fabrication method means that much larger arrays can now be utilised and can be placed on both hemispheres of the brain. In a simulation study using two 57-channel electrode arrays, one on each hemisphere, Aristovich et al. (2016) have shown the potential for EIT to image activity occurring throughout the depth of the rat brain with a localisation accuracy of at least 1 mm.

Somatosensory evoked activity can be generated in response to stimulation of median or tibial nerves and is a useful paradigm for testing the accuracy of EIT. Prior to converging in the cortex, afferents from the medial lemniscal and spinothalamic pathways terminate in the ventral posterolateral nucleus (VPL) in the thalamus (Paxinos, 2014). The VPL receives input from all over the body, however; the region processing forepaw activity is the largest with a volume of between 1.1 mm^3 to 1.4 mm^3 dedicated to this representation (Angel and Clarke, 1975; Parker et al., 1998). Somatosensory activity can be repetitively elicited on demand and their reproducibility is such that they are often used as diagnostic tools in spinal cord injuries and cerebral lesions (Shibasaki et al., 1977; Wang et al., 2017). This is a desirable characteristic as one can take advantage of averaging to increase the signal strength.

The neural connections underlying the somatosensory pathway have been inferred from electrophysiological recordings (Chapin and Lin, 1984; Francis et al., 2008) and histological tract tracing (Bourassa et al., 1995; Erro et al., 2002). Aside from MRI imaging studies that have shown increased blood flow in the pertinent structures (Boussida et al., 2017; Sanganahalli et al., 2013), in-vivo imaging of the trajectory of direct neural activity from the thalamus to the cortex along the somatosensory pathway has not been conducted. If the depth resolution of fast neural EIT can be extended beyond the cortex, it could be used to image the propagation of activity along this pathway.

The purpose of this work was to determine if with two 57-channel electrode arrays placed over both hemispheres on the cortex of an anaesthetised rat, EIT could be used to image ascending neural activity from the VPL nucleus in the thalamus to the cortex during somatosensory forepaw evoked responses. To address this, the impedance change in the thalamus was first characterised directly in terms of magnitude and latency by placing a depth electrode into the VPL nucleus. Subsequently, EIT imaging was conducted in a separate set of experiments that utilised two non-penetrating 57-channel electrode arrays placed on the surface of the cortex. A set of simulations were then performed in order to assess the SNR achieved during imaging experiments and to predict the depth resolution of EIT with epicortical electrodes.

Material and methods

Animal preparation

Six female Sprague-Dawley rats weighing between 300 and 400 g were used in experiments. Anaesthesia was induced in a perspex box using a mixture of isoflurane, O_2 and air. Once anaesthetised a tracheal intubation was performed and anaesthesia maintained with isoflurane (2–2.5%) and a 30/70% mixture of O_2 and air. Depth of anaesthesia was monitored by assessment of the pedal withdrawal and corneal reflexes. Cannulation of the right femoral vessels was then undertaken. The rat was fixed within ear bars in a stereotaxic frame (Narishige International Ltd, UK) and mechanical ventilation using the SAV03 ventilator (Vetronic Services Ltd, UK) commenced. The rats head was shaved, the scalp incised and the temporal muscle cauterized using a bipolar cauterization system (Malis CMC 2, Codman, USA). A craniotomy was performed using a veterinary bone drill (Ideal Micro Drill, US) and the dura removed. The craniotmoy extended from just rostral of lambda down to 4 mm rostral of bregma and laterally along the zygomatic arch. Throughout the craniotomy and upon removal of the skull and dura, the brain was frequently irrigated with warm (38 °C) 0.9% NaCl solution.

To directly characterise the evoked response and impedance changes occurring in the cortex and thalamus the left hemisphere was exposed through a craniotomy and a 57-channel electrode array placed on the exposed cortex. Through a hole in this array, a 16-channel depth electrode was placed in the VPL (ML = 3–3.5 mm, AP = 2.5–3 mm, DV = 5–6 mm). For rats where EIT imaging was conducted, two craniotomies were performed and a 57-channel electrode array was placed on the exposed cortex of each hemisphere.

A 1.5 cm diameter Ag/AgCl reference electrode was placed under the skin at the back of the neck and two silver needle electrodes were placed in the right forepaw for stimulation. Upon completion of surgery, a bolus of 60 $mgkg^{-1}$ of 1% w/v α-chloralose in saline was administered intravenously and then maintained at 20 $mgkg^{-1}$. Throughout the experiment ECG, end tidal C02, respiratory rate, SPO2, mean arterial blood pressure and exhaled gas concentration and were all monitored using the Lightning Vetronics monitor (Vetronic Services Ltd, UK) and kept within the recommended physiological range. The core body temperature of the rat was controlled using a homeothermic heating unit comprising a heating blanket and a rectal probe that provided temperature feedback to the system (Harvard Apparatus, UK). All animal handling and experimental investigations undertaken in this study were ethically approved by the UK Home Office and performed in accordance with its regulations, as outlined in the Animals (Scientific Procedures) Act 1986.

Hardware and electrodes

Data were collected using the ScouseTom EIT system (Avery et al., 2017) with the actiCHamp EEG amplifier (BrainVision, Germany) sampling at 25 kHz. Evoked responses were induced by electrical stimulation of the contralateral forepaw using a Neurolog NL800A (Digimeter, UK) isolated current stimulator. The forepaw was stimulated at a frequency of 2 Hz and 20 Hz using pulses that were 500 μs in duration with a peak amplitude of 10 mA.

To directly characterise the cortical and thalamic responses, a cortical electrode array along with a single shank depth electrode were employed (Fig. 1A). The cortical electrode array was fabricated using a 12.5 μm sheet of stainless steel sandwiched between two layers of silicone. A laser was used to expose 57 × 0.6 mm diameter contacts that had a centre-to-centre spacing of 1.2 mm. The exposed electrode contacts were coated with platinum black prior to placement on the brain in order to reduce contact impedance. The depth electrode (Neuronexus, US) implemented comprised of 16 × 30 μm diameter contacts spanning a length of 1500 μm. Data collected on the depth contacts were passed through a unity gain headstage amplifier (Plexon, TX, USA).

For EIT imaging, two 57-channel cortical electrode arrays were

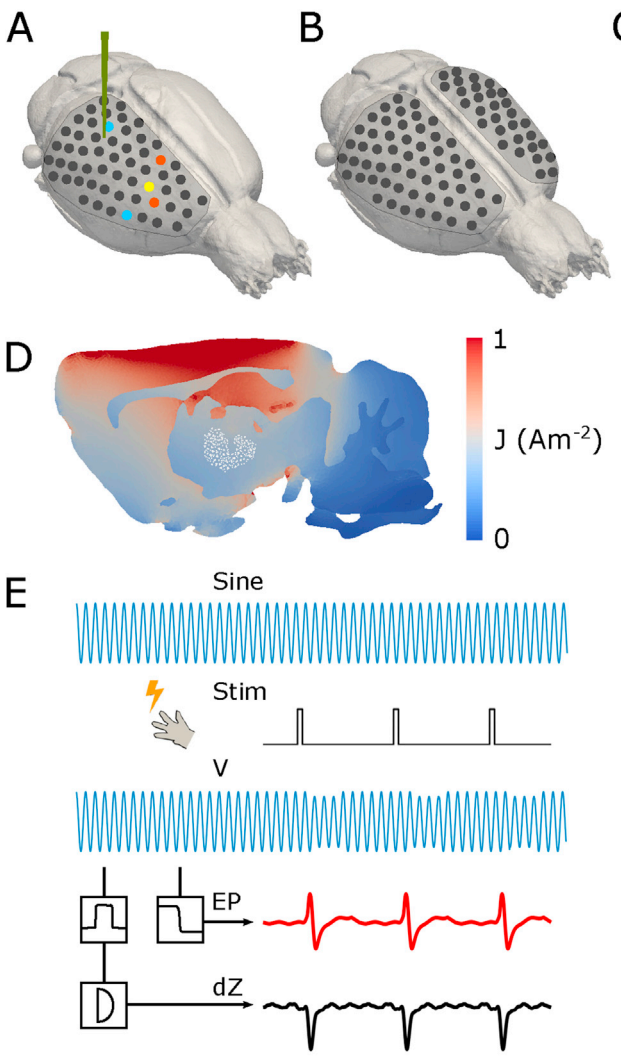

Fig. 1. Experimental setup and data processing. (A) The impedance response in the cortex and thalamus was characterised during forepaw stimulation using a 57-channel electrode array placed on the cortex and a depth electrode placed in the VPL nucleus in the thalamus. Given the location of the maximum evoked potential in the cortex (shown in yellow) an example of a cortical injection pair is displayed in orange. The blue electrodes exhibit an example of an injection pair used to characterise the thalamic response given the location of the depth probe. (B) EIT imaging was conducted in an attempt to image ascending neural activity from the thalamus to the cortex using epicortical electrodes. For these experiments two 57-channel electrode arrays were used, one on each hemisphere of the brain. No depth electrode was implemented. (C) The protocol that maximises current density in the VPL was used for imaging experiments. Given the 114 electrodes implemented, the theoretical protocol consists of 113 independent injection pairs. The first two injection pairs concentrate the most current density into the VPL. (D) The average current density across injection pairs concentrated in a sagittal slice when using the protocol that maximises current density in the VPL. The location of the VPL is highlighted in white (E) Data collection and processing work flow. A sine wave (Sine) of amplitude 50 μA and 1475 Hz was injected between a pair of electrodes and the resulting voltage (V) recorded on the remaining electrodes. The forepaw was stimulated (Stim) to elicit evoked activity. The evoked activity (EP) was extracted from the recorded data by applying a 500 Hz low pass filter. The impedance change (dZ) was found by applying a ±500 Hz bandwidth filter around the carrier frequency and demodulating the filtered signal.

implemented with one placed on each hemisphere of the rat brain. For this set of imaging experiments, no depth electrode was placed in the thalamus.

Data collection and protocols

Single channel impedance measurements were conducted to directly characterise the cortical and thalamic response during forepaw stimulation in terms of latency and magnitude. Characterisation of the impedance signal in the cortex was undertaken using current of amplitude 50 μA and frequency 1475 Hz. Injecting electrode pairs were chosen in the vicinity of the electrode that exhibited the largest evoked potential in order to maximise the sensitivity to cortical activity (Fig. 1A). Thalamic impedance changes were recorded by injecting current through electrodes on the cortical array and measuring the resulting voltages on the depth electrode. For these measurements, the amplitude of injected current was increased to 200 μA and injection pairs were chosen such that current was injected between an electrode located closest to the depth probe and one located furthest away (Fig. 1A). The injection time between a pair of electrodes was 30 s and data were collected for four different injection pairs in N = 3 rats. The forepaw was stimulated at 2 Hz, a frequency where evoked potentials are present in both the cortex and thalamus. The response was additionally characterised at 20 Hz stimulation frequency in view of maximising the number of averages that could be attained in a given time period. At this stimulation frequency, evoked potentials were no longer expected to be present in the cortex but only observed in the thalamus (Brinker et al., 1999; Fokin and Veskov, 1972; Guilbaud et al., 1980; Huttunen et al., 2008).

For EIT imaging experiments current of 50 μA at 1475 Hz was injected. This frequency was chosen as it has been shown to yield the largest impedance response in both the thalamus and cortex (Faulkner et al., 2018). A protocol that maximised the current density in the right hemispherical VPL was used (Fig. 1C and D). This was found by simulating the current density in brain for every possible injection pair and finding the independent set of electrode pairs that maximised the current density in the VPL (Faulkner et al., 2017). To ensure a reasonable recording time for a single imaging dataset, a subset of electrode pairs that concentrated the most current density into the VPL were chosen from the full theoretical protocol which comprised 113 pairs (supplementary figures). The injection time between electrode pairs and the number of injection pairs addressed varied from 60 s to 300 s and 60 to 25 respectively. Full EIT imaging datasets were obtained when stimulating the forepaw at both 2 Hz and 20 Hz. Recordings were obtained in N = 3 rats (Table 1).

Data processing

The recorded voltage measurements contained both the impedance and evoked potential signals. Impedance signals were extracted by applying a ±500 Hz bandpass filter (5th order butterworth) around the carrier frequency and demodulating the signal using the Hilbert transform. The demodulated data was segmented into 500 ms epochs (50 ms

Table 1
Summary of the injection time and the number of electrode pairs used in each rat for EIT imaging experiments when stimulating the forepaw at 2 Hz and 20 Hz.

Rat	Stimulation Frequency (Hz)	Injection Time (s)	No. of injection pairs
1	2	60	60
	20	30	60
2	2	150	30
	20	60	30
3	2	300	25
	20	150	25

for 20 Hz stimulation) that spanned from 250 ms (25 ms) pre-stimulus to 250 ms post-stimulus. The mean of the baseline (200 ms–50 ms (20 ms–5 ms) pre-stimulus) was subtracted from each epoch to express the signal as an impedance change. The epochs were then averaged together yielding a mean impedance change. Injecting, disconnected and noisy channels were removed from further analysis. The latter were defined as channels where the standard deviation of the baseline exceeded 5 μV. Evoked potentials were extracted by applying a 500 Hz low pass filter to the original data. In an analogous way to the impedance change, the low pass filtered data was segmented into epochs and averaged together (Fig. 1E).

To characterise the cortical and thalamic impedance changes, the electrode exhibiting the largest impedance change for each injection pair was considered. The latency at which activity occurs has been evaluated as the time between the stimulation and the first positive peak, in the case of evoked potentials, and the first negative peak for impedance changes.

For the imaging data, impedance changes on all channels for all injection pairs were concatenated together. Time points with significant activity were identified by comparing the signal at each time point across all channels to the signal during the baseline. At each time point a one-sided *t*-test was performed with the significance level set to $\alpha = 0.01$. All data are presented as mean ± S.D.

Image reconstruction

Image reconstruction involved computation of a forward solution and a Jacobian matrix. These were calculated for a given protocol on a 3 million element tetrahedral mesh using the PEITs solver (Jehl et al., 2015) containing grey and white matter and cerebrospinal fluid (CSF) with conductivity values set to 0.3, 0.15 and 1.79 Sm^{-1} respectively (Romsauerova et al., 2006). Electrode positions were altered to match the placement in experiments. Their position relative to the bregma sagittal sinus suture line was recorded and the arrays shifted on the mesh accordingly.

Images were reconstructed every 2 ms on a 150 μm hexahedral mesh. Zeroth order Tikhonov regularisation with noise based correction was used to reconstruct images (Aristovich et al., 2014), with the regularisation parameter chosen at each time point through generalized cross validation. The reconstructed values in each element of the hexahedral mesh represent a t-score (σ) which was calculated by dividing the reconstructed conductivity change in each element by the reconstructed conductivity change in each element due to baseline noise.

For representative images all reconstructions have been thresholded at 25% the maximum reconstructed value occurring at any time point. The centre of mass of activity was calculated after using a threshold of 50%.

Determining the SNR achieved in experiments

The SNR that was achieved during the EIT imaging experiments was estimated in a set of simulations. The aforementioned 3 million element mesh comprising grey matter, white matter and CSF layers with two 57-channel electrode arrays was used to simulate the expected voltage change on the cortical electrodes owing to a conductivity change in the VPL. The simulated perturbation in the VPL was a sphere of volume 1.4 mm^3 with a conductivity change of 0.4% and 0.1%. These parameters were informed by the volume of the forepaw representation in the VPL reported by Angel and Clarke (1975) and the thalamic impedance change measured directly on the depth electrode during the characterisation experiments when stimulating the forepaw at 2 Hz and 20 Hz respectively. Voltage changes were predicted for the protocol that maximised current density in the VPL (Table 2).

After removal of all measurements involving injecting electrodes, the voltage changes were sorted in order of magnitude. The top 1% largest electrode voltage changes were then averaged together. This was taken to be indicative to the size of the impedance change that would be observed in the raw signal on the cortical electrodes. An estimate of the SNR was calculated by dividing this signal with the noise in the experimental imaging data sets. The noise on each channel was taken as the standard deviation of the baseline and an average value obtained by taking the mean across all channels in the data set.

Evaluating realistic depth resolution of EIT in simulations

A second set of simulations were performed to investigate the expected depth accuracy of EIT with cortical electrodes by placing conductivity changes at differing depths within the rat brain mesh. A sphere of volume 1.4 mm^3 with a conductivity change of 0.4% was simulated. The perturbation was placed at the centre of the VPL in the ML and AP axis, (ML = 3.3 and AP = 3) (Paxinos, 2014) and placed at DV positions that spanned from the surface to the bottom of the mesh in 0.5 mm intervals. It was additionally placed in eight other surrounding columns. These were located 1 mm away from the original column in either/both of the ML and AP directions and perturbations also placed at 0.5 mm depth intervals within each column. In total 160 different positions were considered. Realistic additive and multiplicative noise of 0.5 μV and 0.0035% were added to the simulated voltage changes. These values were estimated from experimental data collected after conducting 60 averages; this number of averages was equivalent to injecting between a single electrode pair for 30 s when stimulating at 2 Hz (Table 2).

Zeroth order Tikhonov regularisation with noise based correction was used to reconstruct images with the regularisation parameter chosen through generalized cross validation. All reconstructed images were thresholded at 50% the maximum reconstructed change and the localisation accuracy, localisation error and volume error computed. The localisation error was defined as the distance between the centre of mass of the simulated and reconstructed perturbations. This value was expressed as a percentage by dividing by the average mesh dimension, yielding the localisation error. The volume error was defined as the difference in volume between the simulated and reconstructed perturbation expressed as a percentage of the mesh volume. A successful reconstruction was defined as one where the addition of the localisation and volume

Table 2
Summary of parameters used for simulations to assess the SNR achieved in imaging experiments and the depth sensitivity of EIT when using epicortical electrodes.

	SNR analysis	Depth analysis
Mesh	3 million element tetrahedral	3 million element tetrahedral
Layers	Grey matter White matter CSF	Grey matter White matter CSF
Electrodes	2 × 57 channel array (Fig. 1B)	2 × 57 channel array
Protocol	Max current density in VPL	Max current density in VPL
No. of protocol lines	113	113
Noise	0 μV additive 0% multiplicative	0.5 μV additive 0.0035% multiplicative
Conductivity change	0.4%	0.4%
Volume of change	1.4 mm^3	1.4 mm^3
No. of locations	1	160

errors did not exceed 10%. This threshold was decided based on qualitative inspection of the reconstructed images.

Results

Thalamic and cortical impedance changes

When stimulating the forepaw at 2 Hz, the evoked potentials recorded directly from the VPL nucleus were 266 ± 71 μV at 7.3 ± 2 ms (n = 16 in N = 3). The corresponding impedance change was −0.41 ± 0.14% at 8.8 ± 1.9 ms (Fig. 2B). The peak cortical evoked potential was 1.8 ± 0.8 mV (n = 16 in N = 3) and occurred 12.1 ± 1.6 ms after stimulation. The associated impedance change was −0.16 ± 0.08% in amplitude at 12.9 ± 1.4 ms (Fig. 2E). No significant difference in the latency between the evoked potential and impedance change was observed in the VPL nor the cortex ($p < 0.01$).

When the forepaw was stimulated at 20 Hz, the mean amplitude of the evoked potential measured in the VPL decreased to 168 ± 51 μV (n = 12 in N = 3) and occurred at 6.1 ± 1.5 ms. The corresponding impedance change was −0.1 ± 0.04% at 6.4 ± 0.8 ms (Fig. 2C). At this stimulation frequency, no evoked potential nor impedance change was recorded from the cortex. A significant difference between the evoked potential and impedance change latency was not observed ($p < 0.01$).

EIT imaging data and reconstruction

2 Hz stimulation

After rejection of injecting, disconnected and noisy channels, the number of impedance measurements used for image reconstruction in each rat was 4582 (76% of total), 2845 (83%) and 2173 (74%) respectively. A significant change in the impedance signal was observed between 10.4–21 ms, 11.2–21.8 ms and 10.6–20.6 ms in the three rats respectively. The largest impedance signal observed on any channel in the three rats was −0.15 ± 0.07% at 15 ms, −0.14 ± 0.03% at 15.2 ms and −0.05 ± 0.03% at 15.8 ms respectively (Fig. 3A).

Images were reconstructed every 2 ms over a time period spanning 0 ms–30 ms after stimulation. In the three rats the maximum reconstructed activity occurred between 13 ms–17 ms after stimulation and the centre-of-mass of this activity lay in the S1 forepaw somatosensory cortical area (Fig. 3C). The earliest time point at which a significant

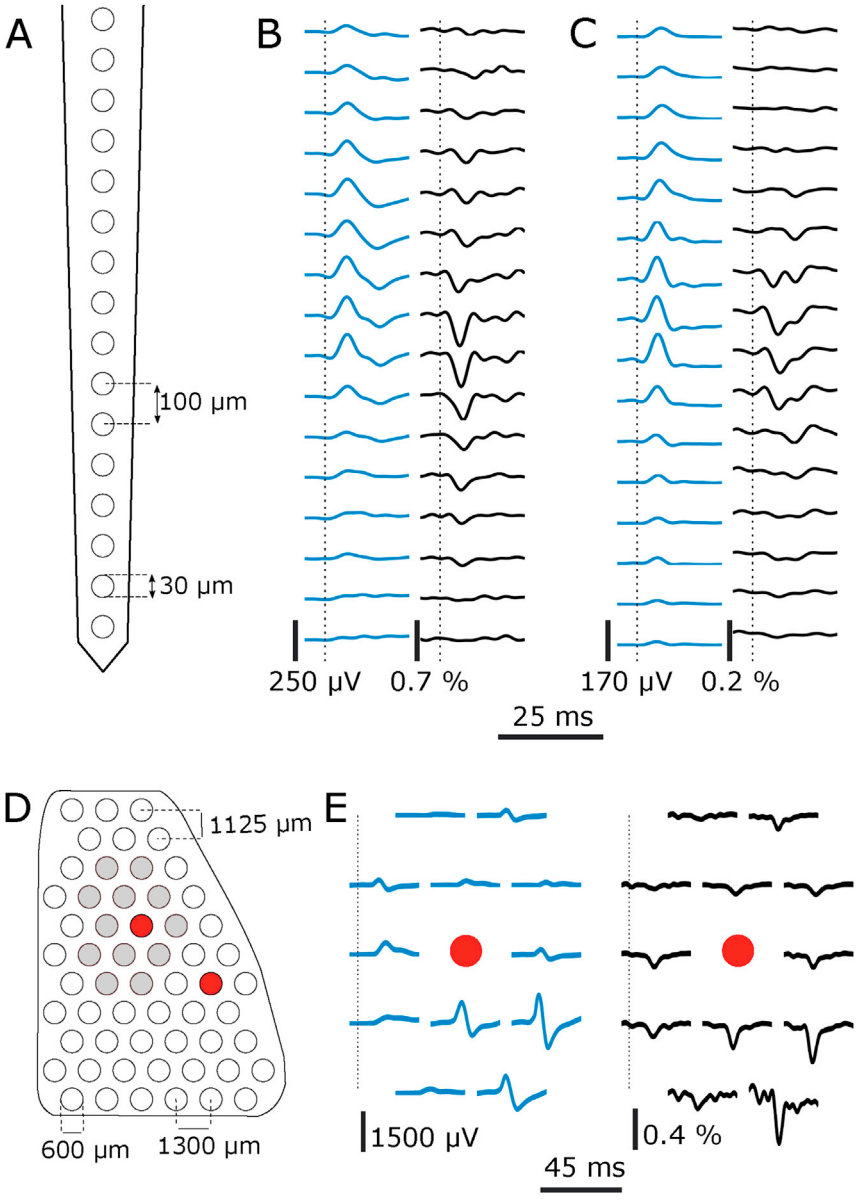

Fig. 2. Thalamic and cortical evoked potentials and impedance changes. (A) Diagram of depth probe used for measurements. (B) Evoked response (first column) and associated impedance change (second column) recorded along the contacts of the probe placed in VPL at 2 Hz forepaw stimulation. Time of stimulation is indicated by dashed line. On the 9th contact down the peak evoked potential was 191.7 μV at 6.0 ms and the impedance change −0.56% at 6.4 ms (C) Evoked response (first column) and associated impedance change (second column) when stimulating at 20 Hz. On the 9th contact down the peak evoked potential was 154.6 μV at 4.6 ms and the impedance change −0.11% at 6.2 ms (D) Diagram of cortical array used for measurements. The electrodes used to inject current are shown in red. Measurements from contacts highlighted in grey are displayed in figure E. (E) Evoked response and associated impedance change recorded from the cortex at 2 Hz forepaw stimulation. Time of stimulation is indicated by dashed line. The largest peak evoked response was 2.5 mV at 12.6 ms with an impedance change of −0.22% at 13.2 ms.

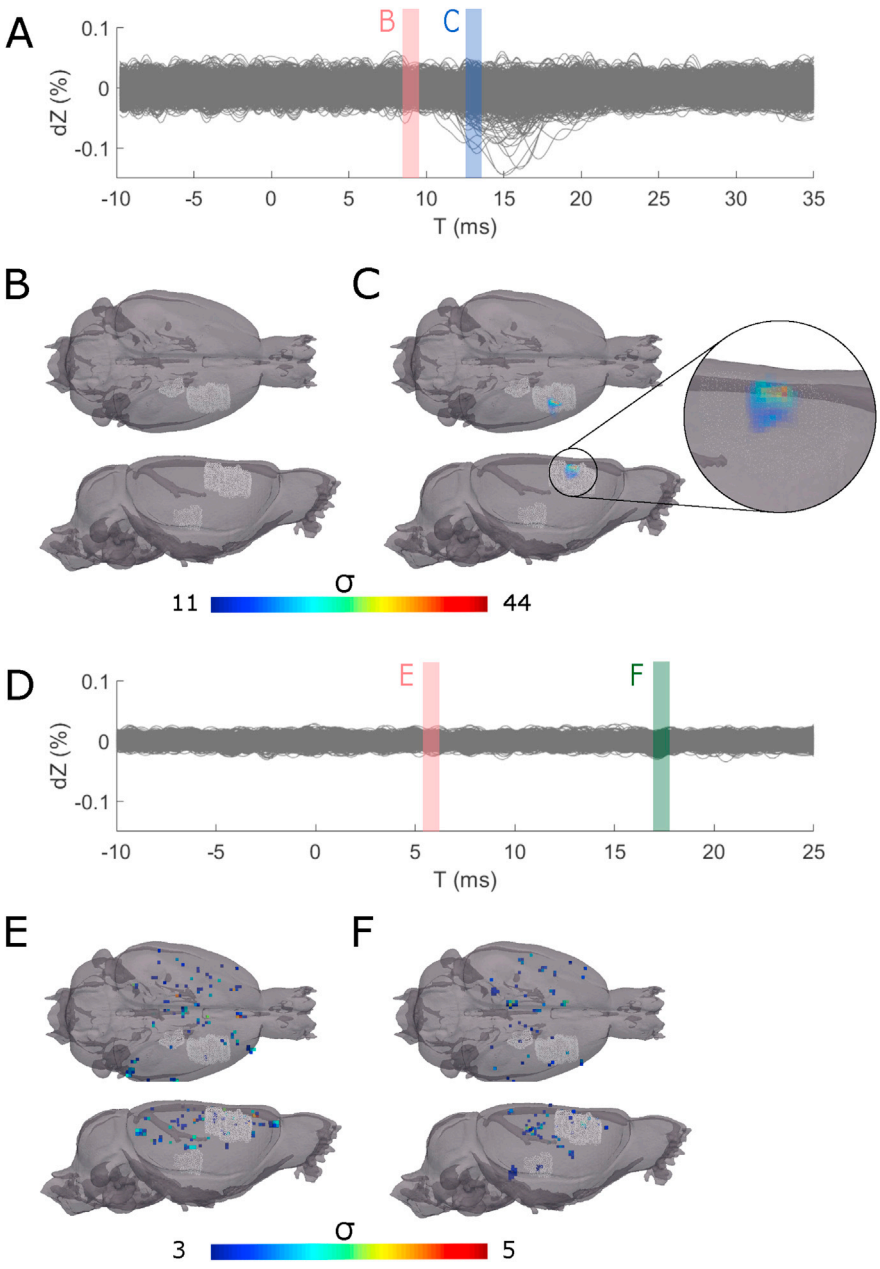

Fig. 3. EIT imaging data and reconstruction for 2 Hz and 20 Hz forepaw stimulation. (A) Example of a complete EIT imaging data set when stimulating the forepaw at 2 Hz. Imaging was undertaken using current of amplitude 50 μA and frequency 1475 Hz. The red bar shows the time at which thalamic activity is expected to occur, 9 ms after stimulation. The blue bar, placed at 13 ms, indicated the expected time of cortical activity. Examples of reconstructions at 9 ms (B) and 13 ms (C) are shown. The location of the VPL and S1 forepaw somatosensory region are outlined in white. At 9 ms no significant activity is observed anywhere in the brain. At 13 ms significant activity is observed in the forepaw somatosensory cortex. (E) Example of an EIT imaging data set when stimulating the forepaw at 20 Hz. The red bar shows the time at which thalamic activity is expected to occur, 9 ms after stimulation. The green bar has been placed at 18 ms and represents a time point where no physiological activity is expected to occur. Examples of reconstructions at 6 ms (E) and 18 ms (F) are shown. Reconstructions at both time points are similarly spread throughout the brain and can not be localised to any structure.

conductivity change was reconstructed in any rat occurred at 12 ms which was after the expected timescale of thalamic activity. No significant activity was reconstructed at a depth below 1.6 mm at any time point in any of the rats.

20 Hz stimulation

The number of impedance measurements used for image reconstruction in each rat when stimulating at 20 Hz was 5745 (84%), 2352 (61%) and 2369 (69%) respectively. In the three rats the earliest time point after stimulation where significant activity was detected in the impedance signal was 0.8 ms, 0.6 ms and 2.6 ms respectively. Based on qualitative inspection, however, no time points where a clear signal distinct from the noise could be observed (Fig. 3D). For completeness, images of this signal were reconstructed; however, the reconstruction could not be localised to any region of the brain and was dominated by small artefactual conductivity changes reconstructed at random locations within the mesh (Fig. 3E and F).

Theoretical SNR based on simulations

When simulating a 0.4% change in the VPL, the mean of the largest 1% of voltage changes on the cortical electrodes was 0.035 ± 0.004 μV. In the three rats the mean noise was 0.81 ± 0.3 μV, 0.67 ± 0.3 μV and 0.41 ± 0.1 μV respectively which yielded SNR's of 0.04, 0.05 and 0.12.

For the 0.1% conductivity change, simulating the 20 Hz stimulation case, the largest expected signal on the cortical electrodes was 0.009 ± 0.001 μV. When considering the mean noise of 0.20 ± 0.08 μV, 0.33 ± 0.14 μV and 0.19 ± 0.07 μV recorded in the three rats, the SNR achieved was 0.045, 0.028 and 0.047 respectively.

Depth resolution of EIT

When considering the average error values across the eight columns considered, perturbations with centres placed more than 2.1 mm below the surface of the cortex had a total error value in excess of 10% (Fig. 4A).

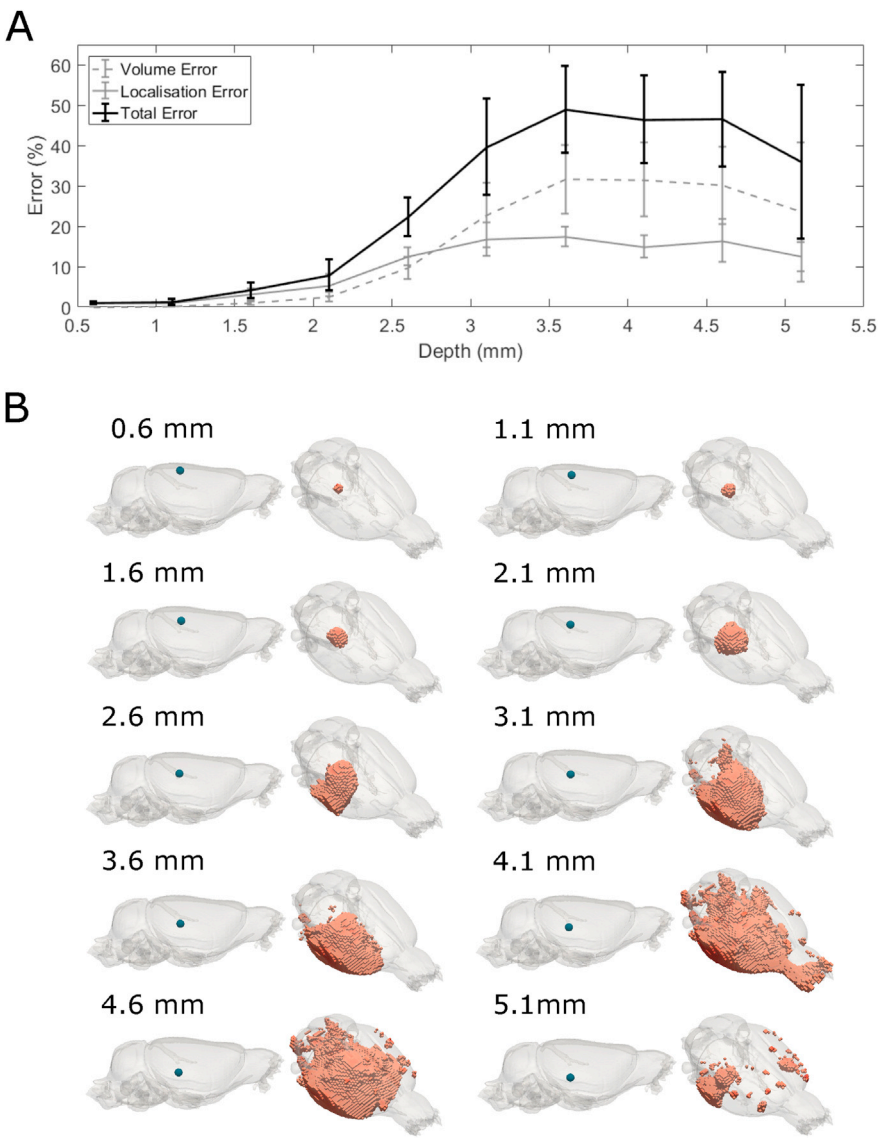

Fig. 4. Simulated depth resolution of EIT. (A) Average volume error, localisation error and total error (mean ± S.D.) for perturbations placed in eight columns at different depths from the surface of the cortex. For perturbations placed at depths greater than 2.1 mm the total error exceeded 10%. (B) Reconstructed images for perturbations with a conductivity change of 0.4% placed at increasing depths from the surface of the cortex in one column. The location and volume of the simulated perturbation are shown in the left mesh in each figure.

From visual inspection, it can be seen that up to 2.1 mm the reconstructed perturbation was spherical and matched the simulated perturbation closely in location (Fig. 4B). The localisation accuracy decreased from 0.10 ± 0.05 mm at depth of 0.6 mm to 0.52 ± 0.2 mm at 2.1 mm below the surface. The reconstruction at a depth 2.6 mm was no longer spherical, however, was still relatively localised. For perturbations placed beyond 3.1 mm, the reconstruction spanned a large volume of the brain. By 4.1 mm the reconstruction was present in most of the brain. The localisation accuracy at the depths ranging from 3.1 mm to 4.1 mm were 2.0 ± 0.1 mm, 2.4 ± 0.1 mm and 1.9 ± 0.1 mm respectively. It was not possible to reconstruct any perturbations whose centre lay below 5.1 mm from the surface of the cortex (Fig. 4B).

Discussion

Summary of results

In this work, impedance changes during evoked forepaw activity occurring in the cortex and VPL thalamic nucleus were characterised. EIT imaging was then conducted using epicortical electrodes in an attempt to track the propagation of somatosensory activity from the thalamus to the cortex. Despite using optimised parameters aimed at detecting thalamic impedance changes, reconstructed activity was confined to the somatosensory forepaw cortical area. Post experimental simulation analysis indicated that the lack of sensitivity to thalamic activity could be attributed to an insufficient SNR and depth accuracy.

Do recorded signals from cortex and thalamus match the literature?

Cortical evoked potentials recorded in this study had an average latency of 12.1 ± 1.6 ms which is consistent with Huttunen et al. (2008), Koyanagi and Tator (1996) and Schwindt et al. (2004) who report cortical evoked potentials occurring between 12 and 17 ms after forepaw stimulation under α-chloralose anaesthesia. There is greater variation in the magnitude of the evoked potential presented in literature which can be attributed to differing recording techniques. Huttunen et al. (2008) measured evoked potentials using a tungsten micro-electrode placed in layer IV of the cortex, perhaps the closest technique to the method used in this study. They observed a mean peak amplitude of 1.3 mV, which is of similar magnitude to the 1.8 ± 0.8 mV recorded in this work.

Previous measurements of cortical impedance changes during evoked activity in the cortex include those undertaken by Aristovich et al. (2016) and Oh et al. (2011); they reported maximum amplitudes of 0.007% and 0.1% respectively. In the current work the cortical impedance change had a larger mean amplitude of -0.16 ± 0.08%. The increased signal observed could be attributed to the excitable properties of α-chloralose

compared to the previously used anaesthesia, halothane (Winters and Spooner, 1966).

Single unit recordings from VPL neurons during forepaw stimulation by (Aguilar et al., 2008) and Angel and Clarke (1975) report response latencies between 5 and 8 ms, which is in agreement with the peak latencies of 7.3 ± 2 ms and 6.1 ± 1.5 ms detected in the VPL when stimulating at 2 Hz and 20 Hz respectively. LFP recordings of forepaw activity stimulated at 0.5 Hz in the VPL by Alonso-Calvino et al. (2016) had an amplitude around 250 μV, a similar amplitude to the 266 ± 71 μV observed here. At 20 Hz stimulation frequency the amplitude of the evoked potential recorded decreased to 168 ± 51 μV. This decrease in amplitude of evoked potential with higher stimulation frequency follows the trend seen by Fokin and Veskov (1972) in their measurements from the VPL. At 2 Hz, they recorded peak evoked amplitudes of around 375 μV, this reduced to 280 μV by 16 Hz and further to 220 μV when stimulating at 32 Hz.

While direct quantification of impedance changes occurring in thalamic nuclei has not previously been undertaken, the detected magnitudes of $-0.41 \pm 0.14\%$ and $-0.1 \pm 0.04\%$ at 2 Hz and 20 Hz respectively match closely with those observed in the cortex. The slightly higher impedance change detected at 2 Hz can be attributed to recording approach. The thalamic impedance change has been measured directly from the centre of the VPL whereas the cortical impedance change has been measured from the surface of the cortex.

Can we image thalamic activity with EIT using cortical electrodes?

In all imaging data sets collected, no signal indicative of a thalamic impedance change was present. When the forepaw stimulation frequency was 2 Hz, the earliest significant time point in any of the three rats occurred 10.4 ms after stimulation. This was later than the expected time course of a thalamic impedance change. The peak impedance changes occurred between 14 ms and 16 ms which is consistent with the latency of the cortical impedance changes measured previously. Reconstructed images localised activity to the S1 forepaw somatosensory region in the cortex in all rats. At 20 Hz stimulation, significant activity was observed as early as 0.6 ms after stimulation. This preceded the expected thalamic impedance change and was likely due to noise. From qualitative inspection no activity distinct from the noise could be observed and this was further confirmed in reconstructed images that did not show any areas of collective activity. Due to time considerations not all injection pairs of the protocol were addressed and this may have influenced the quality of reconstructed images. This was, however, unlikely to have affected the ability to detect thalamic impedance changes as the injection pairs most sensitive to deep activity were prioritised.

Through computation of the theoretical SNR achieved, it became apparent that even the highest number of averages used, 600 (2 Hz for 5 min per injection pair) and 3000 (20 Hz for 2.5 min per injection pair), were insufficient to detect thalamic activity. The respective maximum SNR's achieved at 2 Hz and 20 Hz were 0.12 and 0.047 and thus this explains why no thalamic signal could be seen above the noise. In order to achieve an SNR of three, which has been described by Gilad and Holder (2009) as necessary to conduct EIT imaging, a total of c. 74000 averages would need to be recorded which will likely be practically impossible. This work indicates therefore that imaging thalamic evoked activity from the VPL with EIT when using cortical electrodes is not feasible.

How deep does modelling suggest we can image activity?

In all five columns considered when the centre of the perturbation was placed at a depth below 2.6 mm from the surface of the cortex, the total error exceeded 10%. Beyond depths of 3.1 mm on qualitative inspection the reconstructed volumes were no longer spherical and instead spread throughout the large portions of the mesh. It was not possible to reconstruct images of perturbations placed more than 5.1 mm below the surface of the cortex. Compared to previous simulation studies whose results suggest that EIT can image throughout the rat brain, the lack of depth sensitivity illustrated in these results is somewhat surprising.

When considering the localisation accuracy alone, the results obtained here are not dissimilar from those presented previously by Aristovich et al. (2016). They simulated a conductivity change of 1% and considered only additive noise of 0.5 μV and were able to attain a localisation accuracy of less than 1 mm throughout the brain. It is clear though that consideration of localisation accuracy alone is not a sufficient measure to deem whether a reconstruction is successful or not. While the perturbation located 4.1 mm beneath the surface of the cortex yields a localisation value of 1.9 mm, the reconstruction spans more than half the volume of the brain and it is hard to see how useful physiological information can be obtained from such a reconstruction. By considering the volume as well as the localisation error, we believe a more realistic approach to assessing the depth accuracy of EIT with cortical electrodes has been taken.

Potential applications for epicortical EIT in the rat and in humans

While the depth sensitivity was not sufficient to reach the thalamic structures under consideration in this study, the depth sensitivity of 2.5 mm encompasses roughly the outer third of the rat brain and extends throughout the cortex and into the superficial structures within the hippocampus (Paxinos and Watson, 2013). Epilepsy arises from the hypersynchronous depolarisation of a population of neurons (Bromfield et al., 2006; Margineanu, 2010) and impedance changes during chemically induced epileptic activity as large as 0.3% have been detected with surface electrodes in the cortex (Vongerichten et al., 2016). This magnitude is larger than the 0.13% measured during evoked activity using analogous electrodes. The suggestion is that compared to evoked activity larger local impedance change may be occurring during epilepsy. The hippocampus is highly implicated in epilepsy with the foci often located within this structure (Schwartzkroin, 1994). Given the larger impedance changes anticipated, these simulations suggest that imaging hippocampal epileptic activity may be feasible with cortical electrodes in a rat model.

If these results are translated to a human setting and a similar arrangement of epicortical arrays are implemented, EIT could be expected to image activity in the outer third of the human brain. While such an expansive implantation of electrodes does not commonly occur in humans, subdural grids that can span an area as large as 64 cm^2 are placed on the cortex in epilepsy patients who are considered for resective surgery in order to aid the localisation of the epileptic onset (Behrens et al., 1994; Voorhies and Cohen-Gadol, 2013). The spatial sampling of these grids is typically limited to a 1 cm radius around the electrode (Lachaux et al., 2003). By conducting EIT through these subdural grids, the enhanced depth resolution offered could aid the localisation of foci. Further, unlike EEG detection which is dependent on the orientation of the source, EIT is sensitive to sources oriented in all directions (Witkowska-Wrobel et al., 2018).

Conclusion

The potential to use EIT to image ascending neural activity during forepaw somatosensory evoked activity using electrodes placed on the surface of the cortex of an aneasthetised rat has been investigated. EIT imaging was conducted using parameters aimed at detecting activity in the VPL nucleus of the thalamus. Reconstructed images, however, only displayed activity in the S1 forepaw somatosensory cortex. Simulations using realistic noise and conductivity values derived from experiments indicate that EIT imaging with epicortical electrodes is limited to activity occurring within 2.6 mm of the cortical surface. This work has shown that imaging deep activity such as that arising from the thalamus is not possible using non-penetrating surface electrodes and alternative methods such as the additional implementation of depth electrodes will

be required to gain the necessary depth resolution. EIT with epicortical electrodes may, however, be used to image epileptic activity arising in the hippocampus as the activity is expected to be larger and more superficial.

Acknowledgements

This work was supported by grants from DARPA (N66001-16-2-4066), Blackrock Microsystems and the EPSRC (EP/M506448/1).

Appendix A. Supplementary data

Supplementary data related to this article can be found at https://doi.org/10.1016/j.neuroimage.2018.05.022.

References

Aguilar, J., Morales-Botello, M., Foffani, G., 2008. Tactile responses of hindpaw, forepaw and whisker neurons in the thalamic ventrobasal complex of anesthetized rats. Eur. J. Neurosci. 27, 378–387.
Ahlfors, S.P., Han, J., Belliveau, J.W., Hämäläinen, M.S., 2010. Sensitivity of meg and eeg to source orientation. Brain Topogr. 23, 227–232.
Ahrens, M.B., Orger, M.B., Robson, D.N., Li, J.M., Keller, P.J., 2013. Whole-brain functional imaging at cellular resolution using light-sheet microscopy. Nat. methods 10, 413–420.
Alessandrini, G., Scapin, A., 2017. Depth dependent resolution in electrical impedance tomography. J. Inverse Ill-posed Problems 25, 391–402.
Alonso-Calvino, E., Martinez-Camero, I., Fernandez-Lopez, E., Humanes-Valera, D., Foffani, G., Aguilar, J., 2016. Increased responses in the somatosensory thalamus immediately after spinal cord injury. Neurobiol. Dis. 87, 39–49.
Angel, A., Clarke, K., 1975. An analysis of the representation of the forelimb in the ventrobasal thalamic complex of the albino rat. J. physiology 249, 399–423.
Aristovich, K., Sato Dos Santos, G., Packham, B., Holder, D., 2014. A method for reconstructing tomographic images of evoked neural activity with electrical impedance tomography using intracranial planar arrays. Physiol. Meas. 35, 1095–1109.
Aristovich, K.Y., Packham, B.C., Koo, H., Sato Dos Santos, G., McEvoy, A., Holder, D.S., 2016. Imaging fast electrical activity in the brain with electrical impedance tomography. NeuroImage 124 (Part A), 204–213.
Avery, J., Dowrick, T., Faulkner, M., Goren, N., Holder, D., 2017. A versatile and reproducible multi-frequency electrical impedance tomography system. Sensors 17, 280.
Behrens, E., Zentner, J., Van Roost, D., Hufnagel, A., Elger, C.E., Schramm, J., 1994. Subdural and depth electrodes in the presurgical evaluation of epilepsy. Acta Neurochir. 128, 84–87.
Berényi, A., Somogyvári, Z., Nagy, A.J., Roux, L., Long, J.D., Fujisawa, S., Stark, E., Leonardo, A., Harris, T.D., Buzsáki, G., 2014. Large-scale, high-density (up to 512 channels) recording of local circuits in behaving animals. J. neurophysiology 111, 1132–1149.
Bourassa, J., Pinault, D., Deschênes, M., 1995. Corticothalamic projections from the cortical barrel field to the somatosensory thalamus in rats: a single-fibre study using biocytin as an anterograde tracer. Eur. J. Neurosci. 7, 19–30.
Boussida, S., Traoré, A.S., Durif, F., 2017. Mapping of the brain hemodynamic responses to sensorimotor stimulation in a rodent model: a bold fmri study. PloS one 12 e0176512.
Brinker, G., Bock, C., Busch, E., Krep, H., Hossmann, K.-A., Hoehn-Berlage, M., 1999. Simultaneous recording of evoked potentials and t2*-weighted mr images during somatosensory stimulation of rat. Magnetic Reson. Med. 41, 469–473.
Bromfield, E.B., Cavazos, J.E., Sirven, J.I., 2006. Basic Mechanisms Underlying Seizures and Epilepsy.
Burle, B., Spieser, L., Roger, C., Casini, L., Hasbroucq, T., Vidal, F., 2015. Spatial and temporal resolutions of eeg: is it really black and white? a scalp current density view. Int. J. Psychophysiol. 97, 210–220.
Buzsáki, G., 2004. Large-scale recording of neuronal ensembles. Nat. Neurosci. 7, 446–451.
Chapin, J.K., Lin, C.-S., 1984. Mapping the body representation in the si cortex of anesthetized and awake rats. J. Comp. Neurol. 229, 199–213.
Erro, M.E., Lanciego, J.L., Giménez-Amaya, J.M., 2002. Re-examination of the thalamostriatal projections in the rat with retrograde tracers. Neurosci. Res. 42, 45–55.
Faulkner, M., Hannan, S., Aristovich, K.Y., Avery, J., Holder, D.S., 2018. Characterising the frequency response of impedance changes during evoked physiological activity in the rat brain. Physiol. Meas.
Faulkner, M., Jehl, M., Aristovich, K., Avery, J., Witkowska-Wrobel, A., Holder, D., 2017. Optimisation of current injection protocol based on a region of interest. Physiol. Meas. 38, 1158.
Fokin, V., Veskov, R., 1972. Spatiotemporal characteristics of evoked potentials in the posterior ventrolateral nucleus of the cat thalamus. Neurophysiology 4, 336–342.
Francis, J.T., Xu, S., Chapin, J.K., 2008. Proprioceptive and cutaneous representations in the rat ventral posterolateral thalamus. J. neurophysiology 99, 2291–2304.
Friston, K.J., Bastos, A.M., Pinotsis, D., Litvak, V., 2015. Lfp and oscillationswhat do they tell us? Curr. Opin. Neurobiol. 31, 1–6.
Gilad, O., Holder, D.S., 2009. Impedance changes recorded with scalp electrodes during visual evoked responses: implications for electrical impedance tomography of fast neural activity. Neuroimage 47, 514–522.
Gregoriou, G.G., Gotts, S.J., Zhou, H., Desimone, R., 2009. High-frequency, long-range coupling between prefrontal and visual cortex during attention. science 324, 1207–1210.
Guilbaud, G., Peschanski, M., Gautron, M., Binder, D., 1980. Neurones responding to noxious stimulation in vb complex and caudal adjacent regions in the thalamus of the rat. Pain 8, 303–318.
Helmchen, F., Denk, W., 2005. Deep tissue two-photon microscopy. Nat. methods 2, 932–940.
Hillman, E.M., 2007. Optical brain imaging in vivo: techniques and applications from animal to man. J. Biomed. Opt. 12, 051402–051402.
Hunold, A., Funke, M., Eichardt, R., Stenroos, M., Haueisen, J., 2016. Eeg and meg: sensitivity to epileptic spike activity as function of source orientation and depth. Physiol. Meas. 37, 1146.
Huttunen, J.K., Gröhn, O., Penttonen, M., 2008. Coupling between simultaneously recorded bold response and neuronal activity in the rat somatosensory cortex. Neuroimage 39, 775–785.
Jehl, M., Dedner, A., Betcke, T., Aristovich, K., Klöfkorn, R., Holder, D., 2015. A fast parallel solver for the forward problem in electrical impedance tomography. IEEE Trans. Biomed. Eng. 62, 126–137.
Kajikawa, Y., Schroeder, C.E., 2011. How local is the local field potential? Neuron 72, 847–858.
Klivington, K.A., Galambos, R., 1967. Resistance shifts accompanying the evoked cortical response in the cat. Science 157, 211–213.
Koyanagi, I., Tator, C.H., 1996. The effects of cortical stimulation, anesthesia and recording site on somatosensory evoked potentials in the rat. Electroencephalogr. Clin. Electromyogr. Mot. Control 101, 534–542.
Lachaux, J.P., Rudrauf, D., Kahane, P., 2003. Intracranial eeg and human brain mapping. J. Physiol. Paris 97, 613–628.
Lin, M.Z., Schnitzer, M.J., 2016. Genetically encoded indicators of neuronal activity. Nat. Neurosci. 19, 1142–1153.
Lowet, E., Roberts, M.J., Bonizzi, P., Karel, J., De Weerd, P., 2016. Quantifying neural oscillatory synchronization: a comparison between spectral coherence and phase-locking value approaches. PloS one 11 e0146443.
Margineanu, D.G., 2010. Epileptic hypersynchrony revisited. Neuroreport 21, 963–967.
Nunez, P., Silberstein, R., Cadusch, P., Wijesinghe, R., Westdorp, A., Srinivasan, R., 1994. A theoretical and experimental study of high resolution eeg based on surface laplacians and cortical imaging. Electroencephalogr. Clin. neurophysiology 90, 40–57.
Ogawa, S., Lee, T.-M., Nayak, A.S., Glynn, P., 1990. Oxygenation-sensitive contrast in magnetic resonance image of rodent brain at high magnetic fields. Magnetic Reson. Med. 14, 68–78.
Oh, T., Gilad, O., Ghosh, A., Schuettler, M., Holder, D.S., 2011. A novel method for recording neuronal depolarization with recording at 125–825 hz: implications for imaging fast neural activity in the brain with electrical impedance tomography. Med. Biol. Eng. Comput. 49, 593–604.
Parker, J.L., Wood, M.L., Dostrovsky, J.O., 1998. A focal zone of thalamic plasticity. J. Neurosci. 18, 548–558.
Paxinos, G., 2014. Somatosensory System. Academic press.
Paxinos, G., Watson, C., 2013. In: The Rat Brain in Stereotaxic Coordinates, seventh ed. Elsevier.
Raducanu, B.C., Yazicioglu, R.F., Lopez, C.M., Ballini, M., Putzeys, J., Wang, S., Andrei, A., Rochus, V., Welkenhuysen, M., Helleputte, N. v., et al., 2017. Time multiplexed active neural probe with 1356 parallel recording sites. Sensors 17, 2388.
Romsauerova, A., McEwan, A., Horesh, L., Yerworth, R., Bayford, R., Holder, D., 2006. Multi-frequency electrical impedance tomography (EIT) of the adult human head: initial findings in brain tumours, arteriovenous malformations and chronic stroke, development of an analysis method and calibration. Physiol. Meas. 27, 147–161.
Sanganahalli, B.G., Herman, P., Behar, K.L., Blumenfeld, H., Rothman, D.L., Hyder, F., 2013. Functional mri and neural responses in a rat model of alzheimer's disease. Neuroimage 79, 404–411.
Schwartzkroin, P.A., 1994. Role of the hippocampus in epilepsy. Hippocampus 4, 239–242.
Schwindt, W., Burke, M., Pillekamp, F., Luhmann, H.J., Hoehn, M., 2004. Functional magnetic resonance imaging and somatosensory evoked potentials in rats with a neonatally induced freeze lesion of the somatosensory cortex. J. Cereb. Blood Flow Metabol. 24, 1409–1418.
Shibasaki, H., Yamashita, Y., Tsuji, S., 1977. Somatosensory evoked potentials: diagnostic criteria and abnormalities in cerebral lesions. J. Neurol Sci. 34, 427–439.
Theer, P., Denk, W., 2006. On the fundamental imaging-depth limit in two-photon microscopy. JOSA A 23, 3139–3149.
Velluti, R., K., K., R., G, 1968. Evoked resistance shifts in subcortical nuclei. Curr. Mod. Biol. 2, 78–80.
Vongerichten, A.N., dos Santos, G.S., Aristovich, K., Avery, J., McEvoy, A., Walker, M., Holder, D.S., 2016. Characterisation and imaging of cortical impedance changes during interictal and ictal activity in the anaesthetised rat. NeuroImage 124, 813–823.
Voorhies, J.M., Cohen-Gadol, A., 2013. Techniques for placement of grid and strip electrodes for intracranial epilepsy surgery monitoring: pearls and pitfalls. Surg. Neurol. Int. 4.

Wang, Y., Li, G., Luk, K.D., Hu, Y., 2017. Component analysis of somatosensory evoked potentials for identifying spinal cord injury location. Sci. Rep. 7, 2351.
Winters, W., Spooner, C., 1966. A neurophysiological comparison of alpha-chloralose with gamma-hydroxybutyrate in cats. Electroencephalogr. Clin. neurophysiology 20, 83–90.
Witkowska-Wrobel, A., Aristovich, K., Faulkner, M., Avery, J., Holder, D., 2018. Feasibility of imaging epileptic seizure onset with eit and depth electrodes. NeuroImage 173, 311–321.